2020-01-01

Expression, Purification, And Characterization Of Recombinant Human NPAS2

Brenda Moreno
University of Texas at El Paso

EXPRESSION, PURIFICATION, AND CHARACTERIZATION OF RECOMBINANT HUMAN NPAS2

BRENDA MORENO

Master's Program in Chemistry

APPROVED:

Chuan Xiao, Ph.D., Chair

Mahesh Narayan, Ph.D.

German Rosas-Acosta, Ph.D.

Stephen L. Crites, Jr., Ph.D.
Dean of the Graduate School

EXPRESSION, PURIFICATION, AND CHARACTERIZATION OF RECOMBINANT HUMAN NPAS2

by

BRENDA MORENO, B.S.

THESIS

Presented to the Faculty of the Graduate School of

The University of Texas at El Paso

in Partial Fulfillment

of the Requirements

for the Degree of

MASTER OF SCIENCE

Department of Chemistry

THE UNIVERSITY OF TEXAS AT EL PASO

December 2020

Abstract

Many living organisms have biological clocks known as circadian rhythms that control various physiological and behavioral processes, tailored with the day and night. At the cellular level, the circadian clock drives daily rhythms with a transcriptional-translational feedback loop (TTFL) established by multiple transcription factors and genes under their regulation. Circadian Locomotor Output Cycles Kaput (CLOCK) and Brain and Muscle ARNT-like protein 1 (BMAL1) are two of those transcription factors, initiating the TTFL by forming a heterodimeric complex that bind to DNA promoters. Neuronal PAS domain protein 2 (NPAS2) is a functional analog to CLOCK. Less knowledge about NPAS2, in contrast to CLOCK, is available, hindering our understanding of its roles in the circadian rhythm. To study human NPAS2, large amounts of recombinant protein were expressed in bacterial systems and purified using various liquid chromatography techniques. Dynamic light scattering, circular dichroism, and size-exclusion chromatography were used to characterize the recombinant human NPAS2. Abnormal rhythms attributed to NPAS2 have been associated with mental illnesses and certain types of cancer. The characterization of NPAS2 will deepen our understanding of its functions in the circadian rhythm and will facilitate the design of therapeutic treatments targeting circadian related disorders.

Table of Contents

List of Tables

List of Figures

Chapter 1 Introduction

1.1 The Circadian Rhythm

In many living organisms, the circadian rhythm is an intrinsic biological clock with cycles of approximately 24 hours, which have evolved to the Earth's rotation on its axis. It can be traced back 2.5 billion years to the first simple molecular clock appearing in cyanobacteria[1]. In 1729, French astronomer Jean Jacques d'Ortous de Mairan recorded the first observations of the circadian rhythm in the mimosa plant[2]. Then in the 1930s, German biologist Erwin Bunning measured the leaf movement of a bean plant to an almost 24-hour period synchronized to the day and night. With the help of recombinant DNA technology, the Drosophila *period*[*] was the first circadian gene to be cloned and characterized in the 1970-1980s by Jeffrey C. Hall, Michael Rosbash, and Michael W. Young, independently, leading to the 2017 Nobel Prize in Medicine[2]. More and more circadian genes were later identified and studied, with which a molecular mechanism was proposed as the transcriptional-translational feedback loop (TTFL) (Figure 1.1)[3,4].

The TTFL is formed by a network of transcription factors and genes under their regulation. To start the TTFL, two of those transcription factors, Circadian Locomotor Output Cycles Kaput (CLOCK) and Brain-Muscle ARNT-like protein 1 (BMAL1) heterodimerize. Then, the CLOCK/BMAL1 complex binds to E-Box DNA elements to activate the transcription of many circadian related genes including, *period (Per)* and *cryptochrome (Cry)*. In turn, the accumulation of *Per* and *Cry* mRNA leads to the translation and formation of PER/CRY complexes in the cytosol[5]. After a time-delay to reach a concentration threshold, these complexes translocate to the nucleus to repress the function of CLOCK/BMAL1, inhibiting the transcription of *Per* and *Cry*.

[*] In this thesis, italicized and all-capitalized words will be used to refer to genes and proteins, respectively.

These inhibitions continue during the night until the PER/CRY complexes themselves are sufficiently degraded by an ubiquitin-proteasome system[6]. The TTFL sustains this cycle with a periodicity of approximately 24 hours[7].

In multi-cellular organisms, every individual cell has its own TTFL-controlled circadian rhythm that needs to be synchronized at the body level. In mammals, the master clock is located in the suprachiasmatic nucleus (SCN) of the hypothalamus[8]. This central pacemaker regulates and entrains peripheral clocks with the input of external environmental stimuli known as zeitgebers[8]. The predominant zeitgeber to the master clock is light[9]. Light signals are perceived by photoreceptors in the eye which are then transferred via the retino-hypothalamic tract (RHT) to the SCN[9]. When responding to light signals, the SCN utilizes neurotransmitters to synchronize the circadian rhythms of peripheral cells[10].

Despite many years of circadian rhythm study, the details of its molecular mechanism are still elusive. For example, it is unclear whether DNA binding of CLOCK/BMAL1 occurs rhythmically or if the complex remains bound throughout the entire circadian cycle. The mechanism of how PER/CRY inhibits the function of CLOCK/BMAL1 also requires further investigation. The structures of CLOCK/BMAL1 complexed with DNA[11] and PER complexed with the C-terminal of CRY[12,13] have been determined, which have deepened our knowledge of the molecular mechanism of the circadian rhythm. However, there is no high-resolution structural information on other circadian complexes. Structural and functional studies of the circadian proteins will provide insights and fill the current gap of knowledge.

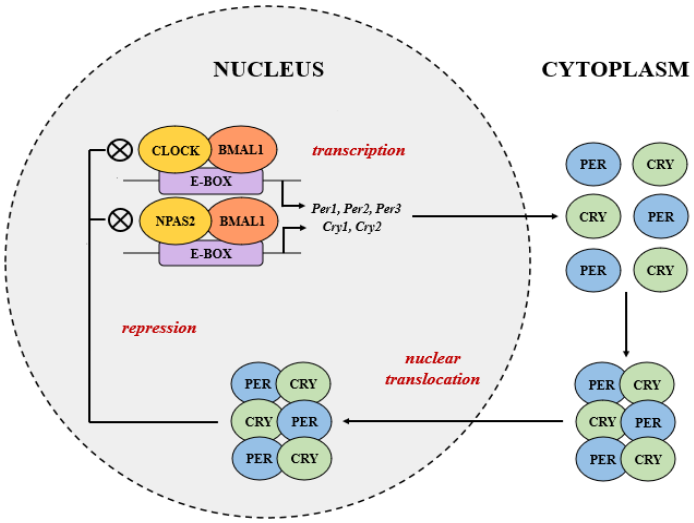

Figure 1.1 The schematic diagram of the transcriptional-translational feedback loop (TTFL). Circadian Locomotor Output Cycles Kaput (CLOCK) or Neuronal PAS domain protein 2 (NPAS2) heterodimerize with Brain-Muscle ARNT-like protein 1 (BMAL1) to induce the transcription of many circadian genes including, three period (*Per1*, *Per2*, and *Per3*) and two cryptochrome (*Cry1* and *Cry2*) genes. In turn, the accumulation of the PER/CRY complexes translocate into the nucleus to repress the function of CLOCK/BMAL1 (or NPAS2/BMAL1).

1.2 The bHLH-PAS Protein Domain

Multiple Per-ARNT-Sim (PAS) domains are found in CLOCK, BMAL1, and PER proteins. The PAS domain consists of ~130 amino acids and has also been observed in signal transduction proteins that sense environmental signals like oxygen, light, voltage, redox potential, and even small toxic aromatic molecules[14,15]. The PAS domain has a conserved structure that comprises of a five-stranded antiparallel β-sheet with several α-helices flanking it (Figure 1.2)[15]. In CLOCK and BMAL1, the DNA-binding regions have additional basic helix-loop-helix (bHLH) domains at the N-terminal regions of their PAS domains. The bHLH-PAS domain is usually found in the N-terminal region of proteins with highly conserved structures whereas the C-terminal regions have various sequences and flexible structures[16].

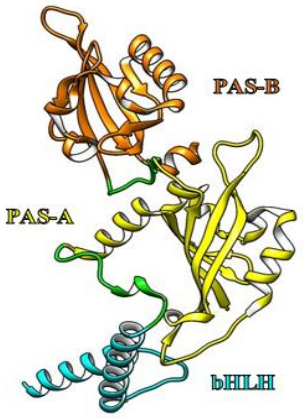

Figure 1.2 The structures of bHLH–PAS domains in murine CLOCK (PDB 4F3L). Murine CLOCK has two PAS domains, denoted as PAS-A and PAS-B. Their structure is presented as a ribbon diagram together with the bHLH domain in the N-terminal region. The bHLH, PAS-A, PAS-B, and linker regions are colored in cyan, yellow, orange, and green, respectively. The ribbon diagram was generated using the UCSF Chimera program[17].

The bHLH-PAS domain has been observed in many proteins with limited structural information on their role in multiprotein complexes[18]. For example, in addition to the CLOCK/BMAL1 complex, the bHLH-PAS domain has also been observed in another heterodimer found in the hypoxia pathway as a response to low oxygen in the cellular environment[18]. This heterodimer is formed between hypoxia inducible factor alpha (HIF-α) and aryl hydrocarbon receptor nuclear translocator (ARNT)[19]. It is noteworthy that both CLOCK/BMAL1 and HIF-α/ARNT bind E-box DNA elements, indicating a common molecular mechanism among different signal-transduction pathways[16,18].

1.3 NPAS2

Neuronal PAS domain protein 2 (NPAS2, also termed MOP4) is another circadian protein that was first characterized in 1997 by Yu-Dong Zhou *et al.* as a mammalian protein, when it was sequenced and added to the bHLH-PAS family[20]. In murine NPAS2, a similar flexible region to the ARNT PAS-B domain has been found in the six-residue long HI loop connecting the Hβ and

Iβ strands. This flexible region has also been observed in Drosophila PER, and in the contact region between CLOCK and CRY proteins[18,21]. Based on sequence homology analysis, NPAS2 was predicted as a functional analog of CLOCK. Furthermore, its classification in the bHLH-PAS family suggested that NPAS2 could serve as a gene regulatory protein like CLOCK[20]. Later, NPAS2 was shown to have a similar function to CLOCK when the circadian rhythmicity in the SCN was maintained in CLOCK-deficient animals[22]. Real-time PCR results have shown that *Npas2* is expressed within the SCN. Without CLOCK, NPAS2 can keep the SCN clockwork maintained with no interference from other brain regions[22].

Interestingly, there has been contradicting results on whether NPAS2 can regulate the circadian rhythm in peripheral tissues or not. Some studies showed that NPAS2 can maintain the circadian clock only in the SCN, while others present results indicating that NPAS2 can substitute CLOCK in peripheral cells in certain tissues[22,23]. A hypothesis regarding why NPAS2 cannot perform its job in other tissues was raised that a molecular ligand with or without its receptor might be present in the SCN that is not found in peripheral clocks or vice-versa[22]. Overall, further investigation is needed to prove or disprove this hypothesis. Also, it is unknown how the overlapping function of NPAS2 with CLOCK helps the master clock in the SCN. It could either be a genetic compensation or simply a redundant mechanism[22]. Others suggested the overlapping roles of both proteins could provide the circadian pathway an ability to function in a tissue specific manner[5].

1.4 Binding to Heme and the Effect of CO on NPAS2 Function

Besides the bHLH-PAS domain, a heme binding motif was observed in NPAS2, which can inhibit the DNA binding of the NPAS2/BMAL1 transcription complex in response to carbon monoxide (CO)[24]. The CO is generated during heme degradation by oxygenases[24]. An *in vitro*

study showed that without CO, NPAS2 and CLOCK can continue DNA binding in the murine liver and promote transcription of E-box-controlled circadian genes (*Per1*, *Per2*, *Cry1*, *Cry2*, and *Rev-erbα*)[25]. While heme is bound to the NPAS2/BMAL1 complex, the increase in concentration of CO dissociates NPAS2 from E-box DNA elements[25]. This suggests that endogenous CO has an interfering role in the regulation of the TTFL[25].

1.5 The Role of NAD and SIRT1

As described in Section 1.4, besides generating CO, heme degradation also consumes NADPH[25]. The reducing cofactors, NADH and NADPH, have been shown to enhance DNA binding of CLOCK/BMAL1 *in vitro*, whereas their oxidized forms have the reverse effects[4]. However, the stronger reducing agent, DTT, did not produce the inhibition, suggesting that NAD works as a molecular ligand rather than changing the redox states[26]. More studies revealed NAD functions as a circadian metabolite by promoting Sirtuin 1 (SIRT1) to interfere with DNA binding[11,27,28]. SIRT1, a nicotinamide adenosine dinucleotide (NAD)-dependent deacetylase, alters the expression of circadian rhythm-associated genes through their deacetylation, including *Bmal1*, *Npas2*, *Clock*, and *Per2*[29,30], thus showing another pathway where NAD can affect the circadian rhythm with or without NPAS2.

1.6 NPAS2 Related Diseases

Sleep deprivation and jetlag caused by circadian rhythm disruption can lead to the degeneration of neurons in the brain[31]. It has also been found that shift workers have developed cognitive impairment, as well as metabolic and mental illness[32]. *Npas2* is highly expressed in brain regions such as the striatum that are responsible to process the reward- and stress-response[33]. Abnormal rhythms attributed to NPAS2 have been linked to psychiatric illnesses like seasonal affective disorder, bipolar disorder, and depression[33].

In addition, *Npas2* could be a potential biomarker for cancers such as colorectal and breast cancer due to its association with tumor initiation and progression[34,35]. Nevertheless, it is unclear how *Npas2* affects cancer cell survival. One study on hepatocellular carcinoma have shown an upregulation of *Npas2* which is believed to facilitate cell survival both *in vitro* and *in vivo*[36]. However, the regulation of *Npas2* expression in cancer is tumor type specific[36].

1.7 Circadian Rhythm Research and Health

Because the circadian rhythm is linked to many pathologies, it is an important therapeutic target in pharmacological research. One focus is to find small molecules that can bind to circadian proteins to alter circadian rhythms[37]. Another approach aims at chrono-pharmacology and its compelling benefits. Some diseases have flares at certain times of the day[7]. Several enzymes and transporter proteins that are involved in drug metabolism show circadian oscillations. Understanding the mechanism behind chrono-pharmacology can help design appropriate time scheduled drug treatments with higher efficacy[38].

As mentioned in Section 1.3, NPAS2 is mainly expressed in the master clock located in the SCN. It is also related to many mental diseases and certain cancers (Section 1.6). The characterization of this circadian regulator holds a great importance. It will uncover essential knowledge about the role of NPAS2 in the SCN and build the foundation for developing therapeutic treatments in circadian related diseases.

1.8 Specific Aims

Aim 1) Expression and purification of recombinant human NPAS2 (hNPAS2)

To characterize hNPAS2, large amounts of homogenous protein is needed. Human *Npas2* has been cloned and expressed in bacterial systems with tags for improving solubility and purification. hNPAS2 was also co-expressed with molecular chaperones to further improve protein folding. Multiple techniques were used to purify the recombinant hNPAS2.

Aim 2) Characterization of recombinant hNPAS2

Recombinant hNPAS2 has been characterized using various biochemical and biophysical techniques, including size exclusion chromatography, dynamic light scattering, and circular dichroism.

Chapter 2 Materials and Methods

2.1 Gene Cloning of *hNpas2* gene into a pColdTF Expression Vector

Gene cloning was carried out by Karla Moriel, a former member of the group. The *hNpas2* gene was codon optimized for bacterial expression by GenScript Biotech with additional codons for 6xHis tag at the 3' end of the gene. The synthesized gene was cloned into a pColdTF vector (Takara Bio USA Inc.) by digestion of both synthesized gene and vector using restriction endonucleases NdeI and XhoI (NEB, cat. #R0111S and R0146S). The digested *hNpas2* insertion was ligated overnight with the vector using T4 DNAse Ligase Reaction Buffer (NEB, cat. #B0202S). The resulting ligated product was transformed into *E. coli* Mach1 (Thermo Fisher, cat. # C862003) competent cells for plasmid purification using the Qiagen Plasmid Purification Kit (Qiagen, cat #12943). The sequence of the plasmid was verified using a DNA sequencer at the Border Biomedical Research Center (BBRC) of The University of Texas at El Paso. The pColdTF expression system includes the bacterial trigger factor (TF) at the N-terminal of the inserted recombinant protein. The TF (48kDa) is a bacterial chaperone that was fused to the recombinant hNPAS2 to facilitate protein folding and solubility, whereas the His tag was included for the affinity purification.

2.2 Co-Transformation with pKJE7

The purified TF-hNPAS2 plasmid was co-transformed with a pKJE7 (Takara, cat. #3340) chaperone plasmid into *E. coli* BL21 (DE3) competent cells (NEB, cat #C2527I). The pKJE7 chaperone plasmid contains genes coding for multiple chaperones, including DNAK (~70kDa), DNAJ (~40kDa), and GRPE (~22kDa). The co-expression of these chaperones was utilized to improve the protein folding of recombinant TF-hNPAS2.

2.3 Expression of recombinant TF-hNPAS2

Individual colonies of the co-transformed cells from Section 2.2 were picked to grow starter cultures in 25ml of TB media (Fisher Scientific, cat. #BP97285) containing 100µg/ml and 34µg/ml final concentration of ampicillin (GoldBio, cat. #A-301) and chloramphenicol (GoldBio, cat. #C-105), respectively. They were incubated overnight for ~14h at 37°C with 260rpm shaking. Large-scale cultures were grown with a 1:200 dilution of starter culture. The media contained 100µg/ml, 34µg/ml, and 1mg/ml final concentration of ampicillin, chloramphenicol, and L-arabinose (GoldBio, cat. #A-300), respectively. L-arabinose was added to the culture as an inducer of the chaperone expression from the pKJE7 plasmid. Once the OD_{600} of 1.0 was reached, the shaking was stopped, and the temperature was reduced to 15°C to activate the transcription using the cold-shock promoter of the pCOLDTF plasmid. Additional L-arabinose was added to increase its final concentration by 1mg/ml. Once the temperature settled to 15°C, the cultures were induced with 1mM IPTG and the shaking was re-started at 260rpm. Protein was expressed for 2h. SDS-PAGE and western blot were used to confirm the expression.

2.4 Purification of Recombinant TF-hNPAS2

2.4.1 Cell Lysis

The bacterial cultures were collected and centrifuged at 4,696xg for 20min. The supernatant was removed, and the pellet was weighed. Each 0.1g of pellet was resuspended in 1ml of lysis buffer (20mM Tris-HCl pH 8.0, 500mM NaCl, 5mM DTT, 10mM $MgCl_2$, and 0.02% NaN_3). Due to the fact that DTT hinders circular dichroism (CD) analyses, it was removed from the buffers in later purifications. After adding PMSF and lysozyme to the final concentration of 1mM and 25µg/ml, respectively, the lysate was incubated at room temperature for 20min with gentle rocking. The lysate was then frozen and stored at -80°C.

Frozen lysate (~200ml) was thawed and additional PMSF was added to increase the final concentration by 1mM. The lysate was sonicated on ice for 4 trials of 7sec with time breaks of 3min. Together with the lysozyme, the sonication further broke the bacterial cell wall to release the recombinant protein. The sample was then incubated with DNase and $MgCl_2$ to the final concentration of 20µg/ml and 10mM, respectively, for 10 minutes. Finally, cell debris was removed by centrifugation at 44,000xg and the supernatant was filtered through 0.2µm filters prior to affinity purification.

2.4.2 Affinity Chromatography

A 5ml HisTrap HP affinity chromatography column (GE, cat. #17371205) was pre-equilibrated with buffer A (20mM Tris–HCl pH 8.0, 500mM NaCl, and 0.02% NaN_3). The lysate of the recombinant TF-hNPAS2 was loaded to the column with a flowrate of 1ml/min. The column was washed with buffer A until the UV absorption stabilized to its lowest value. The column was further washed using a step gradient of 10mM, 20mM, and 40mM imidazole generated by mixing buffer A with buffer B (20mM Tris–HCl pH 8.0, 500mM NaCl, 500mM imidazole, and 0.02% NaN_3) at different ratios. The bound proteins were eluted at 60mM, 120mM and 250mM imidazole generated as mentioned above. These three fractions will be analyzed throughout this thesis as affinity fractions, AF60, AF120, and AF250. Fractions of the purification process were collected and examined with SDS-PAGE.

2.4.3 Anion-exchange Chromatography (AEX)

The PI of TF-hNPAS2 was estimated to be 5.62 using the ExPASy online tool[39], suggesting that the protein will strongly bind to a positively charged resin at pH 8[40]. Therefore, an anion-exchange purification was performed to further purify the recombinant protein. Before the ion-exchange chromatography, the AF60, AF120, and AF250 from the affinity purification were buffer

exchanged to a desalting buffer (20mM Tris-HCl pH 8.0, 100mM NaCl, and 0.02% NaN3) using a HiPrep 26/10 column (Sigma, cat. #17-5087-01). At a flowrate of 1ml/min, the desalted samples from the AF60 and AF120 were combined and loaded to a 5ml HiTrap Q HP anion-exchange column (GE, cat. #17-1153-01) pre-equilibrated with the same desalting buffer. A trial experiment was performed to elute the bound protein using a continuous gradient generated by mixing the desalting buffer with an AEX buffer (20mM Tris–HCl pH 8.0, 1M NaCl, and 0.02% NaN_3) at a continuously changing ratio. From this trial experiment, the recombinant TF-hNPAS2 was observed to mainly elute at a calculated concentration of NaCl between 253mM and 325mM. In the final AEX experiment, the bound protein was eluted in a step-gradient of 253mM, 298mM, and 505mM NaCl, generated with the AEX buffer. These three fractions will be analyzed throughout this thesis as AEX fractions, AEX253, AEX298, and AEX505. Fractions collected were examined on SDS-PAGE and subjected to bicinchoninic acid assay (BCA) (Thermo Scientific, cat. # 23225) to measure the concentration of the protein.

2.5 Characterization of Recombinant TF-hNPAS2

2.5.1 Size-Exclusion Chromatography (SEC)

The molecular weight of recombinant TF-hNPAS2 was analyzed by a Superdex 200 10/300 SEC column (GE, cat. #17-5175-01). The column was pre-equilibrated with SEC buffer (20mM Tris-HCl pH 8.0, 100mM NaCl, 2mM DTT, 10mM $MgCl_2$, and 0.02% NaN_3). For each SEC, 300µl of AF samples without desalting were loaded. The individual peaks were collected and examined by SDS-PAGE.

2.5.2 Dynamic Light Scattering (DLS)

DLS spectra were measured using a Zetasizer Nano S (Malvern) instrument set at 4°C. For each measurement, 500µl of the protein samples were added to disposable cuvettes (Plastibrand, cat. #759075D) with a 1.0cm pathlength. The size data was averaged from 3 cycles of 11 iterations. The sample concentrations were ~0.160mg/ml and ~0.242mg/ml for desalted AF samples and AEX samples, respectively. A separate salt-addition test was performed on the AEX253 sample to test whether adding NaCl would change the size of the recombinant protein. The NaCl concentration was increased to 428mM and 605mM by adding filtered 2M NaCl. These samples were incubated on ice with gentle rocking for 20min before DLS measurement. The sample with 605mM NaCl was left at 4°C for a longer incubation period of 3 days prior to another DLS measurement.

2.5.3 Circular Dichroism (CD)

A J-1500 CD spectrophotometer (JASCO) was utilized to measure far-UV CD spectra of the recombinant TF-hNPAS2. The AEX298 sample was diluted to 149mM NaCl with Tris buffer (20mM Tris-HCl pH 8.0) and concentrated to ~0.46mg/ml (3.3µM). The CD measurement parameters are listed on Table 2.1 and the desalting buffer (Section 2.3.3) was used for the baseline

Table 2.1 Parameters used on the CD spectrophotometer.

Parameters	Values
Measurement Range	190nm – 260nm
Scanning Speed	50nm/min
Data Integration Time	4 sec
Bandwidth	2.0nm
Data Pitch	0.1nm
Accumulation	3
Temperature	4°C

measurement. For the CD measurement, 50µl of the TF-hNPAS2 was added into a clean 0.1mm pathlength quartz cuvette (JASCO, cat. #J/0559). Using the JASCO Spectra Analysis tool, the CD ellipticities (mdeg) were converted to molar ellipticities ($deg \cdot cm^2 \cdot dmol^{-1}$) by providing the cell pathlength, concentration, and number of amino acid residues. The resulting spectra were analyzed with BeStSel[41] and JWMVS-529 CD Multivariate SSE program (JASCO). These programs use default reference sets to deconvolute CD data and elucidate the secondary structure content.

2.5.4 Homology Modeling of TF-hNPAS2

The protein sequence for hNPAS2 was submitted to the I-TASSER structure prediction server[42,43], which provides 5 models from similar templates found in the Protein Data Bank (PDB). The modelled structures were visualized in the UCSF Chimera program[17] and analyzed with the data retrieved from the circular dichroism spectra.

Chapter 3 Results

3.1 The Expression and Purification of TF-hNPAS2

3.1.1 Co-expression of TF-hNPAS2 with Chaperones

The successful co-expression of recombinant TF-hNPAS2 and pKJE7 chaperones in *E. coli* was achieved (Figure 3.1). To produce similar levels of recombinant protein and molecular chaperones, their co-expression was optimized by changing the IPTG concentration, arabinose concentration, expression time, and cell density.

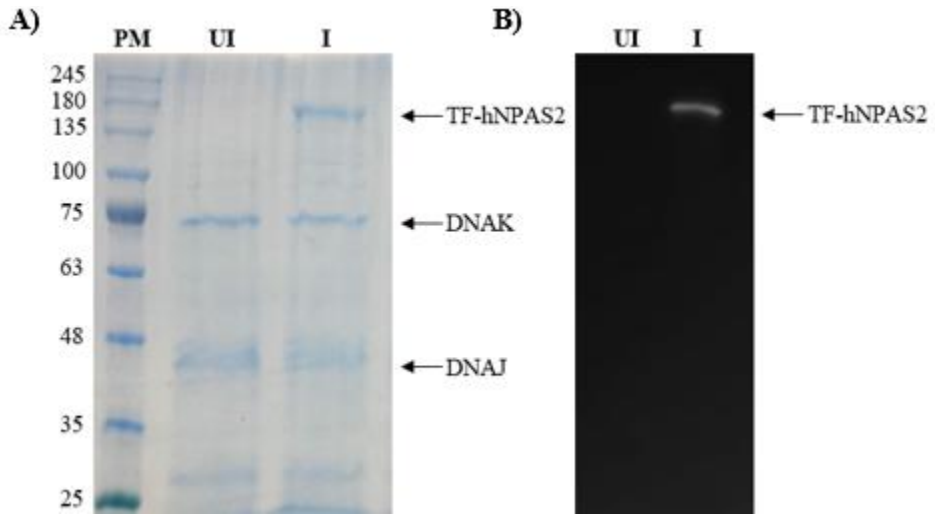

Figure 3.1 Expression optimization of recombinant TF-hNPAS2. A. SDS-PAGE stained by Coomassie. B. Western Blot using anti-His antibodies. Lane 1 in panel A is the protein marker (PM) with kDa labeled on the left. Other lanes in panel A and panel B are uninduced (UI) and IPTG induced (I) samples. Black arrows on the right of both panels point to the expected size of TF-hNPAS2 (~140kDa), DNAK (~70kDa), and DNAJ (~40kDa).

3.1.2 Affinity Purification

The optimized expression of 4L cultures produced enough soluble recombinant TF-hNPAS2 to saturate the 5ml affinity column (Figure 3.2, lane 1 and 2). Most of the contaminants were eliminated in the washes of 10mM, 20mM, and 40mM imidazole (Figure 3.2, lane 3-5). Relatively pure recombinant TF-hNPAS2 were obtained on the 60mM, 120mM, and 250mM

imidazole elutions (Figure 3.2, lane 6-8), which were named AF60, AF120, and AF250 for discussion in the following sections. Based on the molecular weight estimation, the persistent additional band in all elutions was predicted to be the DNAJ chaperone bound to recombinant TF-hNPAS2. This bound chaperone could stabilize the folded state of the protein.

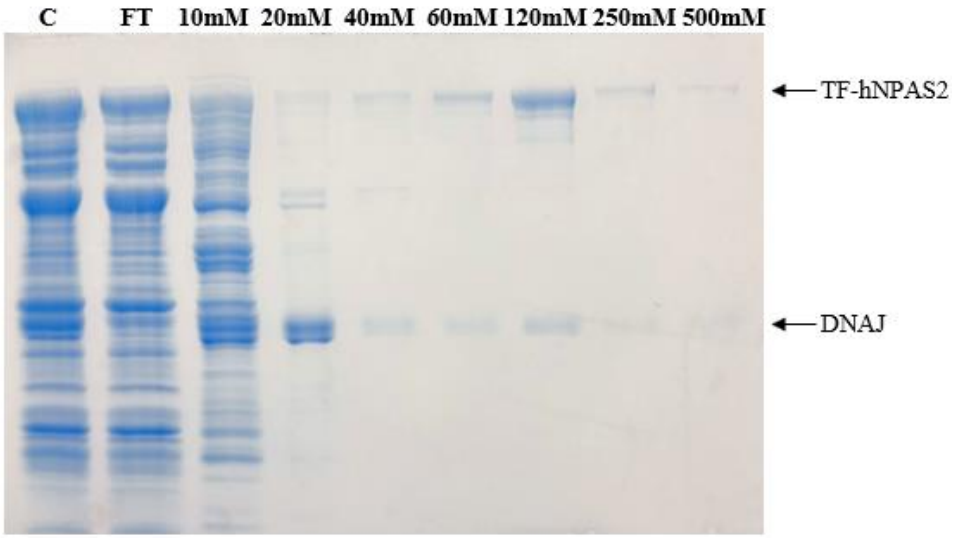

Figure 3.2 SDS-PAGE of affinity purification. Lane 1 and 2 are crude (C) and flow through (FT), respectively. Lane 3 to 9 are fractions from affinity purification with imidazole concentration labeled above the lane. Black arrows on the right point to the expected size of TF-hNPAS2 (~140kDa) and DNAJ (~40kDa).

3.1.3 Anion-Exchange (AEX) Purification

No significant change in purity has been achieved via AEX purification while the predicted DNAJ band is still persistent (Figure 3.3). However, the AEX experiments provide interesting results in further investigations.

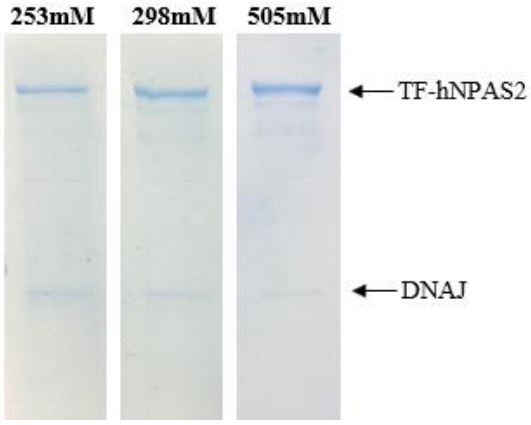

Figure 3.3 SDS-PAGE of AEX purified recombinant TF-hNPAS2. The NaCl concentration is labelled above each lane. Black arrows on the right point to the expected size of TF-hNPAS2 (~140kDa) and DNAJ (~40kDa).

3.2 Characterization

3.2.1 Size-Exclusion Chromatography (SEC)

For the SEC with the AF120 sample, two overlapping peaks were observed on the chromatogram. The first peak at an elution volume of 8.49ml corresponds to an estimated molecular weight of 752kDa, indicating it is a much higher oligomerized form of the recombinant proteins. The second higher peak eluted with an estimated size of 397kDa at the volume of 10.30 ml (Figure 3.4, blue curve). Based on the SEC and SDS-PAGE results, this higher peak could be a dimeric TF-hNPAS2/DNAJ complex. On the contrary, a reversed distribution of the two peaks was observed in the SEC of the AF250 sample where the first peak was much higher than the second peak (Figure 3.4, red curve). This indicates the higher oligomerized form of recombinant proteins are eluted at higher imidazole concentrations in the affinity purification.

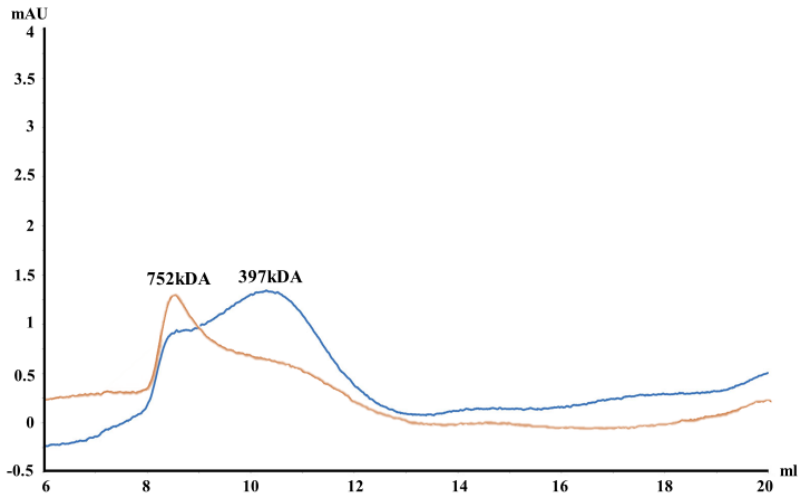

Figure 3.4 SEC chromatogram of TF-hNPAS2 samples. Blue line and orange line are the UV_{280} absorption for the AF120 and AF250 SEC samples, respectively. The estimated molecular weight values were labelled above the two peaks.

3.2.2 Dynamic Light Scattering (DLS)

DLS is a common technique used for measuring hydrodynamic size of macromolecules in solution[44]. Besides providing the hydrodynamic sizes (diameters) of macromolecules at different peak locations in the spectra, the quality of the DLS data can be assessed with multiple parameters[45]. One of these parameters, the polydispersity index (PDI) describes the particle size distribution or homogeneity of a sample[46]. A PDI under 0.1 is highly monodisperse, under 0.3 is nearly monodisperse, and anything over 0.7 is too polydisperse to be a reliable measurement[44,45]. Another parameter, the Y-intercept provides the signal to noise ratio in a DLS measurement[47]. The ideal Y-intercept is 1, but values over 0.6 are considered to be acceptable measurements[47].

Similar peak locations have been observed in the DLS spectra of the affinity purified samples, AF60, AF120, and AF250 (Figure 3.5, Panel A) with an insignificant increase in their size. The estimated hydrodynamic diameters are listed in Table 3.1 together with their quality control parameters, PDI and y-intercept. The PDI of these samples show they are monodispersed. Compared to the affinity purified results, the DLS spectra of the AEX samples, AEX253, AEX298,

and AEX505, show a significant increase in size (Figure 3.5, Panel B). To understand the effect of salt concentration to the size of the complex in the AEX results, a salt-addition test was performed. However, no noticeable differences were observed in this test (Figure 3.6, Table 3.2).

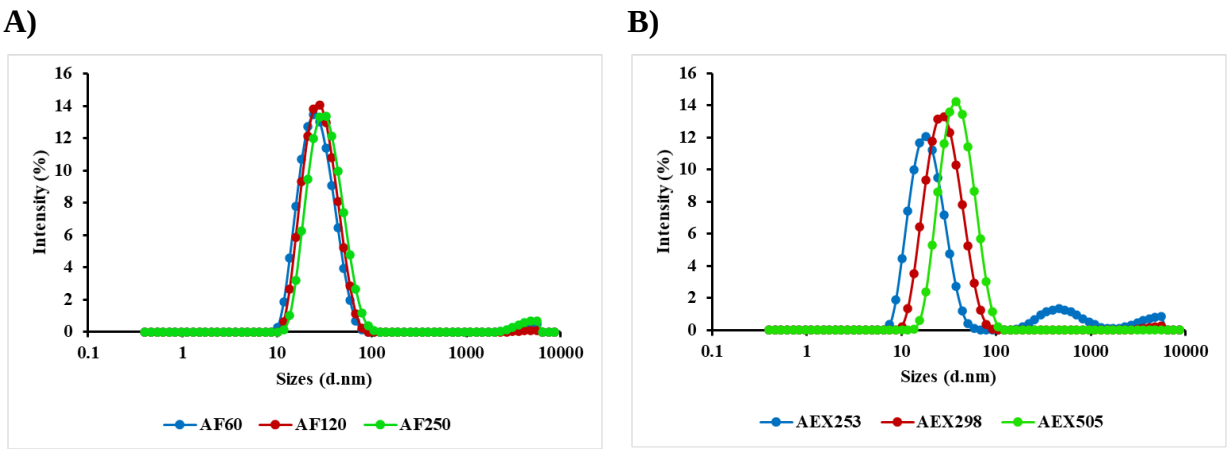

Figure 3.5 DLS spectra on affinity (Panel A) and AEX (Panel B) purified TF-hNPAS2.

Table 3.1 DLS measurement profiles on affinity and AEX purified recombinant TF-hNPAS2.

Samples	AF60	AF120	AF250	AEX253	AEX298	AEX505
PDI	0.188	0.148	0.204	0.374	0.182	0.149
Y-intercept	0.849	0.893	0.894	0.746	0.867	0.883
Peak Location (d.nm)	26.42	28.2	32.51	18.53	28.29	40.30

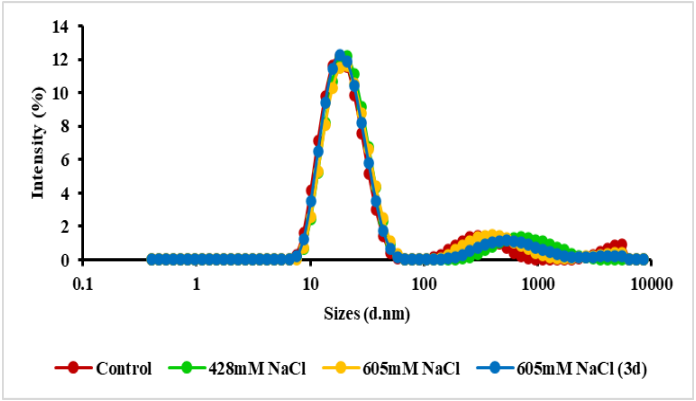

Figure 3.6 DLS spectra of the salt-addition test.

Table 3.2 DLS measurement profiles on the salt-addition test.

Parameters	Control	428mM NaCl	605mM NaCl	605mM NaCl (3d)
PDI	0.336	0.331	0.370	0.336
Y-intercept	0.812	0.716	0.752	0.698
Peak Location (d.nm)	20.32	21.71	22.64	22.33

3.2.3 Circular Dichroism (CD)

The CD spectra of the AEX298 samples are comprised of two troughs between 200-230nm (Figure 3.7). It has been well-established by literature that a 'w'-shaped spectra between 208-222nm contain signals of α-helices whereas a 'v'-shaped spectra between 217-220nm contain signals of β-sheets[48]. The CD spectrum were analyzed by two programs, BeStSel[41] and JASCO's Multivariate SSE, both of which showed a similar proportion of the α-helical, β-sheets, turns, and disordered secondary structures (Table 3.5). The percentage of disordered structures, also known as 'other' or 'irregular' structures, is estimated to be quite high for the AEX298 sample. These disordered structures are difficult to be deconvoluted due to the limitations of computational algorithms[49].

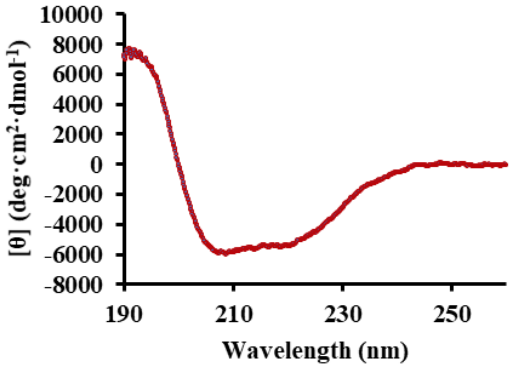

Figure 3.7 CD spectra of the recombinant TF-hNPAS2.

Table 3.3 CD secondary structure estimation by BeStSel and JASCO Multivariate SSE.

	α-helix (%)	β-sheet (%)	Turn (%)	Disordered (%)
BeStSel	13.6	33.8	13.2	39.4
JASCO	18.6	31.2	13.1	37.1

3.2.4 Homology Modelling

No structures of hNPAS2 are available. However, it does have a high sequence homology with murine CLOCK (mCLOCK), whose N-terminal structure of the bHLH-PAS domain has been determined. A BLAST search of the hNPAS2 amino acid sequence showed a 55% identity to mCLOCK over an 83% query coverage. Using homologous structure templates in the PDB, the I-TASSER structure prediction server provides 5 top models, each with a confidence score (C-score). The C-score ranges from -5 to 2, where a higher value indicates a greater confidence in the model[42,43]. Models 1-5 for hNPAS2 received C-scores of 0.65, -2.43, -2.40, -3.15, and -3.30, respectively. It is not surprising that 5 of the top 10 threading templates used by the I-TASSER server for the homology modeling is mCLOCK (PDB 4F3L). The majority of Model 1 has secondary structures that are closely packed into domains leading to its high C-score. The N-terminal of Model 1 contained 31 α-helices bundled in a curved shape (Figure 3.8, Panel A, red part) whereas the C-terminal contained two β-sheet rich domains similar to those observed in the PAS domains (Figure 3.8, Panel A, green part). These two parts are connected by a stretched chain of 14 amino acids (Figure 3.8, Panel A, blue part). Model 2 and 3 each contained a poorly modelled N-terminal domain (Figure 3.8, Panel B and C, red parts). The C-terminal regions of these two models are extended and not well defined, mostly in random coils with very few α-helical content (Figure 3.8, Panel B and C, green parts). It is noteworthy that the mCLOCK structure (PDB 4F3L) could not be superposed with any part of Models 1-3. However, the mCLOCK structure was

superposed well with the N-terminal of Models 4 and 5 with a Cα RMSD less than 1Å across all 319 Cα pairs, even though these two models have lower C-scores (Figure 3.9).

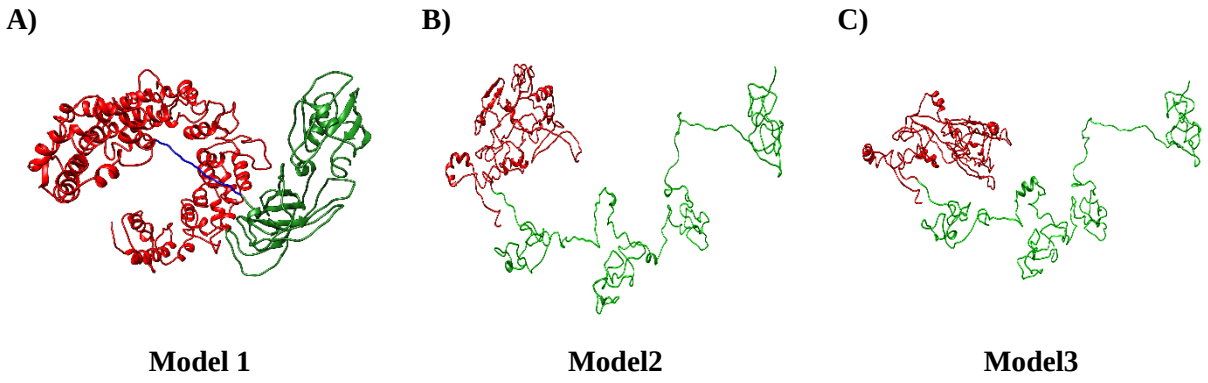

Figure 3.8 Models 1-3 built by the I-TASSER server. All models are shown in ribbon diagrams with the N-terminal and C-terminal colored in red and green, respectively. The ribbon diagram was generated using the UCSF Chimera program[17].

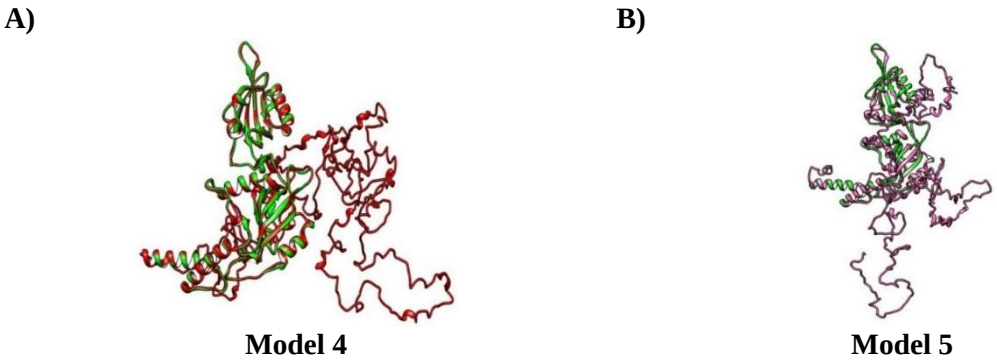

Figure 3.9 Structure comparison between mCLOCK and Model 4 and 5 built by the I-TASSER server. mCLOCK (PDB 4F3L) is superposed to Model 4 (Panel A) and 5 (Panel B). mCLOCK, Model 4, and Model 5 were colored in green, red, and pink, respectively. The ribbon diagram and the superposing were performed using the UCSF Chimera program[17].

Chapter 4. Discussion and Future Work

4.1 Conformational Changes Observed in AEX and SEC

It has been reported that CLOCK and BMAL1 can homodimerize in solution through their individual bHLH domains, however these homodimers are less stable than their heterodimers which are established through the intermolecular contact of PAS domains[11]. Another study of human PER2c also showed multiple oligomeric states displaying different thermal stabilities in solution without the presence of the CRY protein[50]. These results support the two oligomerizations of hNPAS2 observed in the SEC.

The SEC results show that the samples with higher imidazole concentration elute a greater proportion of the larger complex compared to the elutions with lower imidazole concentration. On the contrary, DLS does not show significant size differences of the affinity purified protein complex eluted with different imidazole concentrations. This can be explained by the resolution limit of DLS that might not differentiate the size differences in the two complexes. It can be further supported by the two overlapping peaks in the SEC. Therefore, the sample subjected to the DLS measurement is a mixture of two complexes with different size. The size estimated by DLS is an average from both complexes. Furthermore, the SEC buffers contain DTT which could also affect the oligomerization as seen in a previous study of circadian proteins[50].

When the mixture of desalted AF60 and AF120 were loaded to the AEX column, three distinguished fractions at 253mM, 298mM, and 505mM NaCl with significant size differences were measured by DLS. This further supports that the affinity purified samples are a mixture of different oligomerized TF-hNPAS2/DNAJ with different surface charges. The salt-addition test

demonstrates no transformation between these different oligomers, indicating they might be cross-linked, as suggested in another study of circadian protein, hPER2c[50].

4.2 CD Results and Homology Modelling

The far-UV CD data estimated the majority of the recombinant protein do not have secondary structure content, consistent with 4 of the 5 homology models provided by the I-TASSER server. The C-terminal of these 4 models are largely unstructured indicating there is no reliable template to build the model.

4.3 Conclusion and Future Work

So far, very few structures are available for circadian rhythm proteins, due to the fact that they are dynamic regulatory factors with a high possibility of containing flexible structures. Unfortunately, the structure determination of full-length circadian proteins will be challenging and time consuming. In this study, recombinant TF-hNPAS2 was successfully expressed with molecular chaperones. The protein was purified and characterized using different techniques. SEC and DLS data showed purified recombinant protein might have different oligomerization. CD and homology modelling indicate the C-terminal regions of hNPAS2 might be flexible without secondary structures.

All the results mentioned above will pave the way for future investigations, including the SEC of AEX purified samples with or without DTT. It would also be interesting to study tag-less hNPAS2 using CD and DLS. This will require digestion trials and further purification to remove the TF tag. Because hNPAS2 is a DNA-binding protein, a heparin column can be used for its purification or for DNA-binding assays using E-box elements. Purified hNPAS2 with high homogeneity can also be subjected to structural studies using X-ray crystallography or Cryo-EM.

Determination of the 3D structure of hNPAS2 will provide much-needed information to understand its role in the TTFL. Knowledge about the molecular mechanism of the circadian rhythm will facilitate the development of therapeutic strategies against related diseases.

References

(1) Mazzoccoli, G.; Vinciguerra, M.; Carbone, A.; Relógio, A. The Circadian Clock, the Immune System, and Viral Infections: The Intricate Relationship Between Biological Time and Host-Virus Interaction. *Pathogens* **2020**, *9* (2), 83.

(2) Huang, R. The Discoveries Of Molecular Mechanisms For The Circadian Rhythm: The 2017 Nobel Prize In Physiology Or Medicine. *Biomed. J.* **2018**, *41* (1), 5–8.

(3) Glossop, N.R.J.; Lyons, L.C.; Hardin, P. E. Interlocked Feedback Loops Within the Drosophila Circadian Oscillator. *Science (80-.).* **1999**, *286* (5440), 766–768.

(4) Wulund, L.; Reddy, A. B. A Brief History of Circadian Time: The Emergence of Redox Oscillations as a Novel Component of Biological Rhythms. *Perspect. Sci.* **2015**, *6*, 27–37.

(5) Mcintosh, B. E.; Hogenesch, J. B.; Bradfield, C. A. Mammalian Per-Arnt-Sim Proteins in Environmental Adaptation. *Annu. Rev. Physiol.* **2010**, *72* (1), 625–645.

(6) Zhang, J.; Chatham, J.C.; Young, M. E. Circadian Regulation of Cardiac Physiology: Rhythms That Keep the Heart Beating. *Annu. Rev. Physiol.* **2020**, *82*, 79–101.

(7) Maury, E. Off the Clock: From Circadian Disruption to Metabolic Disease. *Int. J. Mol. Sci* **2019**, *20* (7), 1597.

(8) Reick, M.; Garcia, J. A.; Dudley, C. NPAS2: An Analog of Clock Operative in the Mammalian Forebrain. *Science (80-.).* **2001**, *293* (5529), 506–509.

(9) Bellet, M. M.; Sassone-Corsi, P. Mammalian Circadian Clock and Metabolism - the Epigenetic Link. *J. Cell Sci.* **2010**, *123* (22), 3837–3848.

(10) Ono, D.; Honma, K.; Yanagawa, Y.; Yamanaka, A.; Honma, S. Role of GABA in the Regulation of the Central Circadian Clock of the Suprachiasmatic Nucleus. *J. Physiol. Sci.* **2018**, *68*, 333–343.

(11) Wang, Z.; Wu, Y.; Li, L.; Su, X. Intermolecular Recognition Revealed By The Complex Structure Of Human CLOCK-BMAL1 Basic Helix-Loop-Helix Domains With E-Box DNA. *Cell Res.* **2012**, *23* (2), 213–224.

(12) Nangle, S.N.; Rosensweig, C.; Koike, N.; Tei, H.; Takahashi, J.S.; Green, C.B.; Zheng, N. Molecular Assembly of the Period-Cryptochrome Circadian Transcriptional Repressor Complex. *Elife* **2014**, *3*, 3674.

(13) Schmalen, I. .; Reischl, S. .; Wallach, T.; Klemz, R.; Grudziecki, A.; Prabu, J. R. .; Benda, C. .; Kramer, A.; Wolf, E. Interaction of Circadian Clock Proteins CRY1 and PER2 Is Modulated by Zinc Binding and Disulfide Bond Formation. *Cell* **2014**, *157* (5), 1203–1215.

(14) Dioum, E. M.; Rutter, J.; Tuckerman, J. R.; Gonzalez, G.; Gillez-Gonzalez, M. A.; McKnight, S. L. NPAS2: A Gas-Responsive Transcription Factor. *Science (80-.).* **2002**, *298* (5602), 2385–2387.

(15) Möglich, A.; Ayers, R. A.; Moffat, K. Structure and Signaling Mechanism of Per-ARNT-Sim Domains. *Structure* **2009**, *17* (10), 1282–1294.

(16) Wu, D.; Rastinejad, F. Structural Characterization of Mammalian BHLH-PAS Transcription Factors. *Curr. Opin. Struct. Biol.* **2017**, *43*, 1–9.

(17) Pettersen, E.F.; Goddard, T.D.; Huang, C.C.; Couch, G.S.; Greenblatt, D.M.; Meng, E.C.; Ferrin, T. E. UCSF Chimera--a Visualization System for Exploratory Research and Analysis. *J Comput Chem.* **2004**, *25* (13), 1605–1612.

(18) Card, P. B.; Erbel, P. J.; Gardner, K. H. Structural Basis of ARNT PAS-B Dimerization: Use of a Common Beta-Sheet Interface for Hetero- and Homodimerization. *J. Mol. Biol.* **2005**, *353* (3), 664–677.

(19) Wu, D.; Potluri, N.; Lu, J.; Kim, Y.; Rastinejad, F. Structural Integration in Hypoxia-Inducible Factors. *Nature* **2015**, *524* (7565), 303–308.

(20) Zhou, Y.-D.; Barnard, M.; Tian, H.; Li, X.; Ring, H. Z.; Francke, U.; Shelton, J.; Richardson, J.; Russell, D. W.; Mcknight, S. L. Molecular Characterization of Two Mammalian BHLH-PAS Domain Proteins Selectively Expressed in the Central Nervous System. *Proc. Natl. Acad. Sci.* **1997**, *94* (2), 713–718.

(21) Huang, N.; Chelliah, Y.; Shan, Y.; Taylor, C.; Yoo, S.; Partch, C.; Green, C.; Zhang, H.; Takahashi, J. Crystal Structure of the Heterodimeric CLOCK:BMAL1 Transcriptional Activator Complex. *Science (80-.).* **2012**, *337* (6091), 189–194.

(22) Debruyne, J. P. Oscillating Perceptions: The Ups and Downs of the CLOCK Protein in the Mouse Circadian System. *J. Genet.* **2008**, *87* (5), 437–446.

(23) Landgraf, D.; Wang, L. L.; Diemer, T.; Welsh, D. K. NPAS2 Compensates for Loss of CLOCK in Peripheral Circadian Oscillators. *PLOS Genet.* **2016**, *12* (2).

(24) Kaasik, K.; Lee, C. C. Reciprocal Regulation of Haem Biosynthesis and the Circadian Clock in Mammals. *Nature* **2004**, *430* (6998), 467–471.

(25) Minegishi, S.; Sagami, I.; Negi, S.; Kano, K.; Kitagishi, H. Circadian Clock Disruption by Selective Removal of Endogenous Carbon Monoxide. *Sci. Rep.* **2018**, *8* (1).

(26) Rutter, J.; Reick, M.; Wu, L. C.; McKnight, S. L. Regulation of Clock and NPAS2 DNA Binding by the Redox State of NAD Cofactors. *Science (80-.).* **2001**, *293* (5529), 510–514.

(27) Keshvari, M.; Nejadtaghi, M.; Hosseini-Beheshti, F.; Rastqar, A.; Patel, N. Exploring The Role Of Circadian Clock Gene And Association With Cancer Pathophysiology. *Chronobiol. Int.* **2019**, *37* (2), 151–175.

(28) Asher, G.; Gatfield, D.; Stratmann, M.; Reinke, H.; Dibner, C.; Kreppel, F.; Mostoslavsky, R.; Alt, F.; Schibler, U. SIRT1 Regulates Circadian Clock Gene Expression Through PER2 Deacetylation. *Cell* **2008**, *134* (2), 317–328.

(29) Gaspar, L.; Álvaro, A.; Carmo-Silva, S.; Mendes, A.; Relógio, A.; Cavadas, C. The Importance Of Determining Circadian Parameters In Pharmacological Studies. *Br. J. Pharmacol.* **2019**, *176* (16), 2827–2847.

(30) Chang, H.; Guarente, L. SIRT1 Mediates Central Circadian Control In The SCN By A Mechanism That Decays With Aging. *Cell* **2013**, *153* (7), 1448–1460.

(31) Musiek, E.; Holtzman, D. Mechanisms Linking Circadian Clocks, Sleep, And Neurodegeneration. *Science (80-.).* **2016**, *354* (6315), 1004–1008.

(32) Jagannath, A.; Taylor, L.; Wakaf, Z.; Vasudevan, S.; Foster, R. The Genetics Of Circadian Rhythms, Sleep And Health. *Hum. Mol. Genet.* **2017**, *26* (2), 128–138.

(33) Ozburn, A. R.; Kern, J.; Parekh, P. K.; Logan, R. W.; Liu, Z.; Falcon, E.; Becker-Krail, D.; Purohit, K.; Edgar, N. M.; Huang, Y.; Mcclung, C. A. NPAS2 Regulation of Anxiety-Like Behavior and GABAA Receptors. *Front. Mol. Neurosci.* **2017**, *10*.

(34) Xue, X.; Liu, F.; Han, Y.; Li, P.; Yuan, B.; Wang, X. . et al. Silencing NPAS2 Promotes Cell Growth and Invasion in DLD-1 Cells and Correlated with Poor Prognosis of Colorectal Cancer. *Biochem. Biophys. Res. Commun.* **2014**, *450* (2), 1058–1062.

(35) Yi, C.; Mu, L.; Rigault de la Longrais, I.A.; Sochirca, O.; Arisio, R.; Yu, H.; Hoffman, A.E.; Zhu, Y.; Katsaro, D. The Circadian Gene NPAS2 Is a Novel Prognostic Biomarker for Breast Cancer. *Breast Cancer Res. Treat.* **2010**, *120*, 663–669.

(36) Yuan, P.; Li, J.; Zhou, F.; Huang, Q.; Zhang, J.; Guo, X.; Lyu, Z.; Zhang, H.; Xing, J. NPAS2 Promotes Cell Survival of Hepatocellular Carcinoma by Transactivating

CDC25A. *Cell Death Dis.* **2017**, *8* (3).

(37) Sultan, A. Identification and Development of Clock-Modulating Small Molecules – an Emerging Approach to Fine-Tune the Disrupted Circadian Clocks. *Biol. Rhythm Res.* **2019**, *50* (5), 769–786.

(38) Chen, M.; Zhou, C.; Zhang, T.; Wu, B. Circadian Clock-Controlled Drug Metabolism and Transport. *Xenobiotica* **2020**, *50* (9), 1052–1063.

(39) Gasteiger, E.; Hoogland, C.; Gattiker, A.; Duvaud, S.; Wilkins, M.R.; Appel, R.D.; Bairoch, A. Protein Identification and Analysis Tools on the ExPASy Server. *John M. Walk. Proteomics Protoc. Handb.* **2005**.

(40) Ion exchange chromatography http://tools.thermofisher.com/content/sfs/brochures/TR0062-Ion-exchange-chrom.pdf.

(41) Micsonai, A.; Wien, F.; Kernya, L.; Lee, Y.H.; Goto, Y.; Réfrégiers, M.; Kardos, J. Accurate Secondary Structure Prediction and Fold Recognition for Circular Dichroism Spectroscopy. *PNAS* **2015**, *112* (24), E3095–E3103.

(42) Yang, Y. ; Zhang, Y. I-TASSER Server: New Development for Protein Structure and Function Predictions. *Nucleic Acids Res.* **2015**, *43*, 174–181.

(43) Zhang, C.; Freddolino, P.L.; Zhang, Y. COFACTOR: Improved Protein Function Prediction by Combining Structure, Sequence and Protein–Protein Interaction Information. *Nucleic Acids Res.* **2017**, *45*, 291–299.

(44) Stetefeld, J.; McKenna S.A.; Patel, T. R. Dynamic Light Scattering: A Practical Guide and Applications in Biomedical Sciences. *Biophys. Rev.* **2016**, *8* (4), 409–427.

(45) Danaei, M.; Dehghankhold, M.; Ataei, S.; Hasanzadeh Davarani, F. ; Javanmard, R. . D.; Mozafari, A.; Khorasani, S.; Mozafari, M. R. Impact of Particle Size and Polydispersity

Index on the Clinical Applications of Lipidic Nanocarrier Systems. *Pharmaceutics* **2018**, *10*, 57.

(46) Kaszuba, M. Dynamic Light Scattering https://www.sysmex.nl/fileadmin/media/f102/MLS/Academy_docs/Malvern_Dynamic_Light_Scattering.pdf.

(47) DYNAMIC LIGHT SCATTERING COMMON TERMS DEFINED http://www.biophysics.bioc.cam.ac.uk/wp-content/uploads/2011/02/DLS_Terms_defined_Malvern.pdf.

(48) Ranjbar, B.; Gill, P. Circular Dichroism Techniques: Biomolecular and Nanostructural Analyses- A Review. *Chem. Biol. Drug Des.* **2009**, *74* (2), 101–120.

(49) Whitmore, L.; Wallace, B. A. Protein Secondary Structure Analyses from Circular Dichroism Spectroscopy: Methods and Reference Databases. *Biopolymers* **2007**, *89* (5), 392–400.

(50) Xian, Y.; Moreno, B.; Miranda, V.; Vijay, N.; Nunez, L.C.; Choi, J.; Quinones, C.S.; Rios, P.; Chauhan, N.; Moriel, K.V.; Ruelas, N.J.; Castaneda, A.E.; Rodriguez, R.C.; Amezaga, B.N.; Azzam, S.Z.; Xiao, C. Thermal Stability Analyses of Human PERIOD-2 C-Terminal Domain Using Dynamic Light Scattering and Circular Dichroism. *PLoS One* **2020**.

Vita

After receiving an Associate's degree with honors at EPCC, Brenda Moreno transferred to UTEP for a Bachelor's degree in Biochemistry with the Chemistry department. She joined Dr. Xiao's structural biochemistry lab in the Spring 2017 semester as an undergraduate student and in the Summer 2017 semester, Moreno received the Campus Office of Undergraduate Research Initiatives (COURI) Summer Undergraduate Research Program Assistantship award. She later presented her work at the COURI Summer Symposium at UTEP. She then received the Research Initiative for Scientific Enhancement award for the following school year, Fall 2017/Spring 2018. She travelled to San Diego, California to present her research at the Experimental Biology meeting as member of the American Society for Biochemistry and Molecular Biology. Upon graduation, Moreno was awarded the Undergraduate Award for Academic and Research Excellence in Biochemistry.

As a graduate student in the Master's program, Moreno was a TA and RA in the Chemistry and Biochemistry department and was awarded the Dodson Research grant by the UTEP graduate school. She also presented her work at the American Society for Virology conference in Minneapolis, Minnesota. She will be graduating with her Master's degree in Chemistry in December 2020.

Contact Info: bmoreno4@miners.utep.edu